

SPECIAL ISSUE RESEARCH ARTICLE

Shortening of apparent transverse relaxation time of inorganic phosphate as a breast cancer biomarker

Wybe J.M. van der Kemp | Tijl A. van der Velden | Alexander M. Schmitz |
Kenneth G. Gilhuijs | Peter R. Luijten | Dennis W.J. Klomp | Jannie P. Wijnen

Department of Radiology, University Medical Center Utrecht, Utrecht, The Netherlands

Correspondence

Wybe J. M. van der Kemp, Department of Radiology, University Medical Center Utrecht, P.O. Box 85500, 3508 GA Utrecht, The Netherlands.

Email: w.j.m.vanderkemp@umcutrecht.nl

Funding information

Alpe d'Huzes, Grant/Award Number: UU2013-6302; Nederlandse Organisatie voor Wetenschappelijk Onderzoek, Grant/Award Number: VENI-JW-016.148.002

Phosphorus MRS offers a non-invasive tool for monitoring cell energy and phospholipid metabolism and can be of additional value in diagnosing cancer and monitoring cancer therapy. In this study, we determined the transverse relaxation times of a number of phosphorous metabolites in a group of breast cancer patients by adiabatic multi-echo spectroscopic imaging at 7 T. The transverse relaxation times of phosphoethanolamine, phosphocholine, inorganic phosphate (P_i), glycerophosphocholine and glycerophosphatidylcholine were 184 ± 8 ms, 203 ± 17 ms, 87 ± 8 ms, 240 ± 56 ms and 20 ± 10 ms, respectively. The transverse relaxation time of P_i in breast cancer tissue was less than half that of healthy fibroglandular tissue. This effect is most likely caused by an up-regulation of glycolysis in breast cancer tissue that leads to interaction of P_i with the GAPDH enzyme, which forms part of the reversible pathway of exchange of P_i with gamma-adenosine tri-phosphate, thus shortening its apparent transverse relaxation time. As healthy breast tissue shows very little glycolytic activity, the apparent T_2 shortening of P_i due to malignant transformation could possibly be used as a biomarker for cancer.

KEYWORDS

^{31}P , 7 T, breast cancer, glycolysis, MRSI, transverse relaxation time

1 | INTRODUCTION

Phosphorus magnetic resonance spectroscopic imaging (^{31}P MRSI) enables non-invasive measurement of phospholipid membrane metabolism and cell energy metabolism in vivo. It is well established that enhanced levels of phosphomonoesters (PMEs)—phosphocholine (PC) and phosphoethanolamine (PE)—are a metabolic hallmark of cancer,¹ because these metabolites are key intermediates in phospholipid synthesis, which is enhanced in cancer. Metabolite ratios of PME to phosphodiester (PDE), namely glycerophosphocholine (GPC) and glycerophosphoethanolamine (GPE),² PME to inorganic phosphate (P_i)^{3,4} and PME to gamma-adenosine tri-phosphate (γ -ATP)² have been proposed as biomarkers to assess response to cancer therapy.

Another metabolic hallmark of cancer is up-regulated aerobic glycolysis,⁵ also known as the Warburg effect. Within the glycolytic pathway Steps 6 and 7 involve P_i and these steps are fully reversible⁶ reactions (Figure 1). In Step 6, catalyzed by the enzyme glyceraldehyde-3-phosphate dehydrogenase (GAPDH), glyceraldehyde-3-phosphate is converted into 1,3-diphosphoglycerate (1,3-DPG) by attaching P_i . In Step 7, the reaction

Abbreviations: 1,3-DPG, 1,3-diphosphoglycerate; AMESING, adiabatic multi-echo spectroscopic imaging; ATP, adenosine tri-phosphate; EDTA, ethylenediaminetetraacetic acid; GAPDH, glyceraldehyde-3-phosphate dehydrogenase; GPC, glycerophosphocholine; GPE, glycerophosphoethanolamine; GPTC, (diacyl-)glycerophosphatidylcholine; GPE, (diacyl-)glycerophosphatidylethanolamine; MRSI, magnetic resonance spectroscopic imaging; PC, phosphocholine; PCr, phosphocreatine; PDE, phosphodiester; PE, phosphoethanolamine; PGK, phosphoglycerate kinase; P_i , inorganic phosphate; PME, phosphomonoester

This is an open access article under the terms of the Creative Commons Attribution License, which permits use, distribution and reproduction in any medium, provided the original work is properly cited.

© 2018 The Authors. *NMR in Biomedicine* published by John Wiley & Sons Ltd.

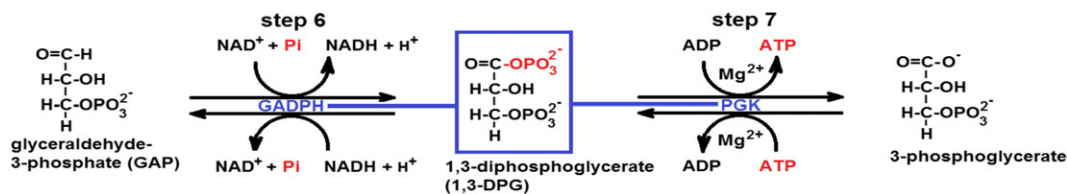


FIGURE 1 The reversible Steps 6 and 7 of the glycolytic pathway involving P_i. The reaction intermediate 1,3-DPG is channelled between the GAPDH and PGK enzymes, without being released into the aqueous environment^{7,8}

product 1,3-DPG is converted to 3-phosphoglycerate under the influence of phosphoglycerate kinase (PGK). Additionally, the phosphate group is transferred to ADP in Step 7. From kinetic modelling⁷ and fluorescence energy transfer measurements,⁸ it has become evident that the enzymes GAPDH and PGK form a loosely bound complex and the intermediate metabolite 1,3-DPG is directly transferred from one enzyme to the next without being released into the aqueous environment.

Effectively, P_i is reversibly exchanged with γ-ATP via this two-step process, which can lead to a substantial line broadening of the P_i signal, i.e. a shortening of its apparent transverse relaxation time, as the maximum enzymatic capacities of GAPDH and PGK can be several hundreds of millimoles per minute per kilogram of tissue, depending on the tissue at hand.⁹

While *in vivo* metabolite ratios measured by MRS should be interpreted carefully, because of their dependence on the combination of flip-angle, repetition time and intrinsic longitudinal relaxation time of the metabolites, measured apparent T_2 values of metabolites can be compared readily and can provide information about the mobility of metabolites. It is well known, for instance, that the large PDE peaks observed at low field in the human breast are mainly from mobile phospholipids and not from aqueous GPC and GPE. However, also at 7 T, mobile phospholipids are the main contribution to the PDE signal in the breast as based on the short apparent T_2 of these signals.¹⁰

Here we show in a group of breast cancer patients an apparent shortening of the transverse relaxation time of the P_i signal, as compared with fibroglandular breast tissue of healthy volunteers, which could well be caused by a mobility restriction on P_i by enzymatic interaction with GAPDH. Additionally, to rule out pH dependence or the effect of general P_i-protein interactions on the transverse relaxation time of P_i, we quantify these influences on the T_2 of P_i solutions in phantom measurements.

2 | METHODS

2.1 | *In vivo* measurements

A group of 24 patients (age range 47–71; average age 59) with breast cancer (identified by the hyperintense area of the dynamic contrast enhanced MRI series and confirmed by histopathology of biopsy from the lesion) comprising 28 lesions (lesion size ≤2 cm; 26 invasive ductal carcinomas, 2 invasive lobular carcinomas) were scanned on a whole-body 7 T MR system (Philips, Best, The Netherlands) with a dual tuned unilateral breast coil. The scan protocol consisted of basic imaging and ³¹P MRSI with an adiabatic multi-echo sequence (AMESING) that was implemented on the scanner as a software patch that has been described in detail elsewhere,¹¹ with $T_R = 6$ s, $\Delta T_E = 45$ ms, matrix $8 \times 8 \times 8$, field of view $160 \times 160 \times 160$ mm³, acquiring one FID and five full echoes with spherical k -space sampling, BW = 8200 Hz and 256 data points for the echoes. The pulse durations of the adiabatic half passage (AHP) and the BIR-4 refocusing pulses that were used in the multi-echo sequence were 2 and 8 ms, respectively; the applied power level was $\gamma B_1 = 1700$ Hz. The center frequency of the pulses was at 4.2 ppm, in between the PDE and PME resonances. At the applied power level the 95% excitation bandwidth of the AHP pulse is 12 ppm and the 95% refocused component of the BIR-4 180 pulse is 9 ppm, causing a maximum of 5% modulation in odd-even echoes that should not affect the T_2 calculation. The TR is 6 s, which is close to the optimal for PMEs, PDEs and P_i (optimal $T_R = 1.25 T_1$). The total scan time of the ³¹P MRSI acquisition was 25 min with one sample average. The study was approved by the medical ethical committee of the University Medical Centre Utrecht and all patients gave written informed consent to participate in the study.

2.2 | Phantom measurements

Six 100 mL phantoms containing 20mM NaH₂PO₄/Na₂HPO₄ in 140mM NaCl and 0.4mM Na₂EDTA in the pH range 6.5 to 7.5 were measured with the same adiabatic multi-echo sequence as was used for the patients. The complexing agent ethylenediaminetetraacetic acid (EDTA) was added to the solutions to minimize the effect of trace metal contamination on the line width of P_i. After the phantoms were measured with ³¹P MRSI, egg albumen (fresh egg white) was added to the solutions amounting to 5 vol.%, and after measurement of the pH (MeterLab PHM210, Radiometer, Copenhagen, Denmark) the albumen P_i solutions were measured again with ³¹P MRSI. The solutions remained clear and stable over the course of the experiments.

2.3 | Analysis of *in vivo* data

Acquired ³¹P MRSI data were processed with home built IDL software. Data were spatially Hanning filtered, apodized (10 Hz Lorentzian) and zero filled to 2048 data points. Spectra were zeroth- and first-order phased and the baselines of the FID spectra were corrected by fitting a second-

order spline. Per subject, data from one or more voxels encompassing the tumor(s) were taken. The spectra (FID and echoes) of the different patients were referenced and aligned to the α -ATP of the FID spectrum and summed to patient group data leading to one summed FID spectrum and five summed echo spectra. All tumor sizes were smaller than the nominal voxel size, and standard voxel shifting (over x , y or z performed in k -space by a linear change of phase on k_x , k_y or k_z respectively) was used to select the tumor volume within one voxel. The group data were spectrally fitted in JMRUI¹² using the AMARES¹³ algorithm with the following a priori constraints: 0.50 ppm chemical shift difference between PE and PC, and 0.56 ppm chemical shift difference between (glycerophosphatidylethanolamine (GPtE) + GPC) and glycerophosphatidylcholine (GPtC).¹⁴ Line widths for PE, PC and P_i were free but identical and line widths for γ -NTP and α -NTP were also free but identical. T_2 fits of the different ³¹P metabolites were made and breast cancer ³¹P spectra and metabolite T_2 values were compared with spectra and metabolite T_2 values of healthy fibroglandular tissue, which were determined in a previous study.¹⁴

2.4 | Analysis of phantom data

Acquired ³¹P MRSI data were Hanning filtered, apodized (10 Hz Lorentzian) and zero filled to 2048 data points. The FID and echo spectra of individual measurements at the various pH values were fitted in JMRUI¹² using AMARES¹³ algorithms and the T_2 of P_i was fitted mono-exponentially.

3 | RESULTS

The FID spectra and the echo spectra of the patient group and the healthy volunteer group¹⁴ are shown in Figure 2A and 2B respectively. The spectra are scaled to the same intensity of P_i in the FID. Note the high PE and PC signals as compared with P_i and PDEs in the breast cancer spectra, while in the healthy spectra PE and PC are lower relative to these signals. Also note the high PDE signals around 2.5 ppm in the summed FID spectrum that drops in intensity with the first echo time of 45 ms (breast cancer as well as healthy tissue). The phosphocreatine (PCr) peak intensity at 0 ppm is somewhat higher in the patient spectra than in the healthy volunteer spectra, because on average the tumor voxels are closer to the pectoralis muscle, with high PCr intensity, than the voxels that were chosen in the healthy volunteers, where we tried to minimize this contamination.

In the spectra of healthy tissue the P_i signal is by far the highest and this remains the case also in the echoes, while in the breast cancer spectra the signal intensity of P_i drops even below the PME signal intensities in the later echoes.

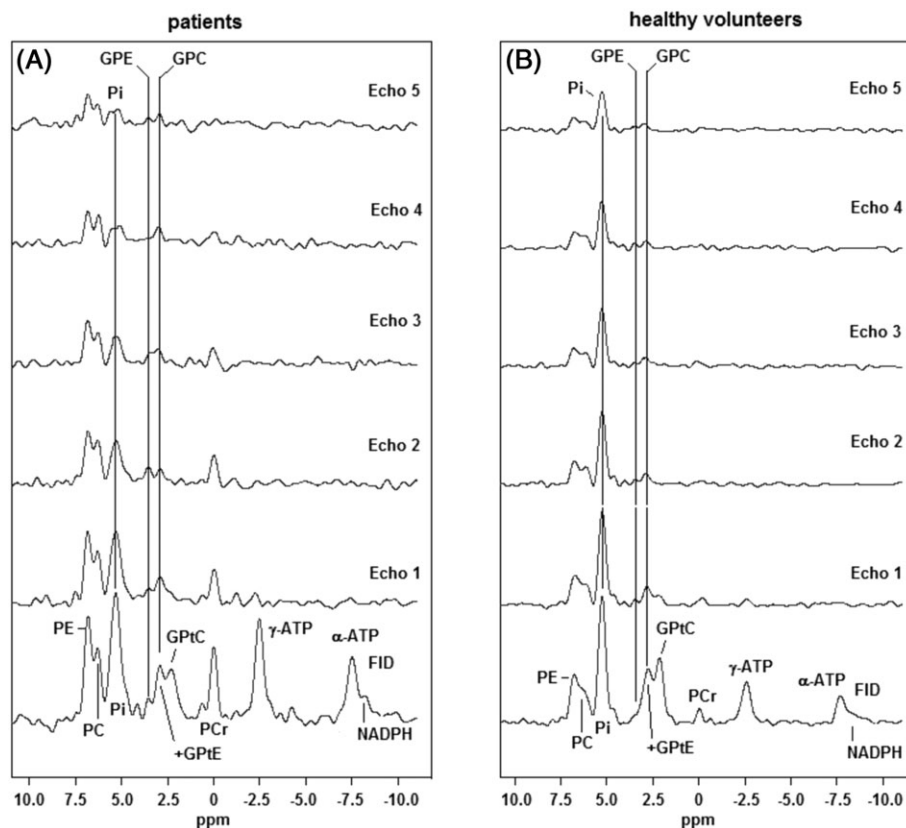


FIGURE 2 Summed FID and echo ³¹P MR spectra of 28 breast cancer lesions of a group of 24 patients (A) and of fibroglandular breast tissue of 8 healthy volunteers (B).¹⁴ Note that the P_i signal in the breast cancer spectrum drops below the PME signals in the later echoes, while in the healthy spectrum it remains the highest signal throughout all echoes

GPtC that were fitted for breast cancer tissue were 184 ± 8 ms, 203 ± 17 ms, 87 ± 8 ms, 240 ± 56 ms and 20 ± 10 ms, respectively. Figure 3 shows fitted T_2 values of various ^{31}P metabolites in breast cancer tissue as a function of those in healthy fibroglandular tissue. There is a substantial difference in the T_2 values of P_i , which are more than twice as long in healthy volunteers as in patients.

Figure 4 shows a direct comparison of the T_2 fits for P_i in breast cancer tissue and healthy fibroglandular tissue. Breast cancer tissue shows a transverse relaxation time for P_i of 87 ± 8 ms, whereas the value in healthy fibroglandular breast tissue is 180 ± 4 ms. The error bars in Figure 4 are based on the quality of the spectral fitting (Cramer-Rao bounds) with AMARES of the (FID and echo) P_i signals.

The influence of pH and added protein (egg albumen) on the T_2 of in vitro P_i solutions is shown in Figure 5A and 5B, respectively.

As can be seen from Figure 5A and 5B, only a small increase ($\sim 15\%$) in T_2 is observed when pH increases from 6.8 to 7.45. Addition of protein tends to dampen this effect.

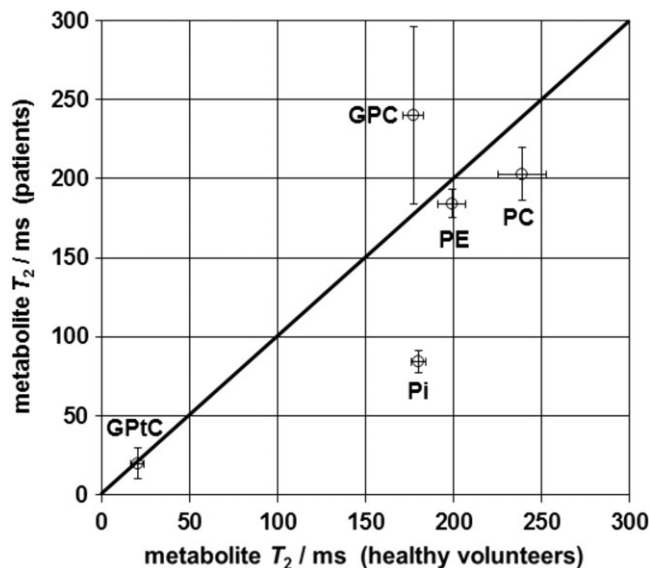


FIGURE 3 Fitted T_2 values of some selected ^{31}P metabolites in breast cancer tissue versus fitted values in healthy fibroglandular tissue. Overall, the T_2 values of the ^{31}P metabolites in breast cancer tissue line up well with those in healthy volunteers, obtained previously,¹⁴ apart from P_i

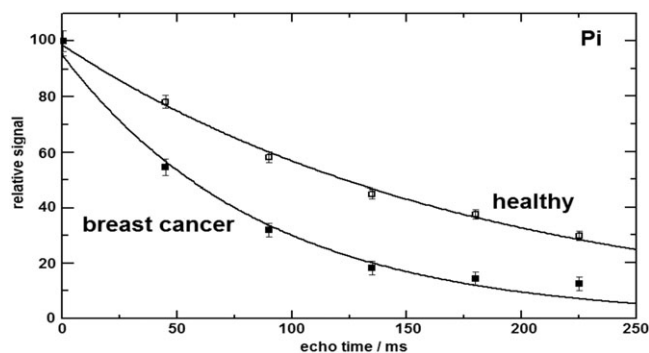


FIGURE 4 Fitted transverse relaxation curves of P_i in breast cancer tissue, $T_2 = 87 \pm 8$ ms, and healthy fibroglandular breast tissue, $T_2 = 180 \pm 4$ ms

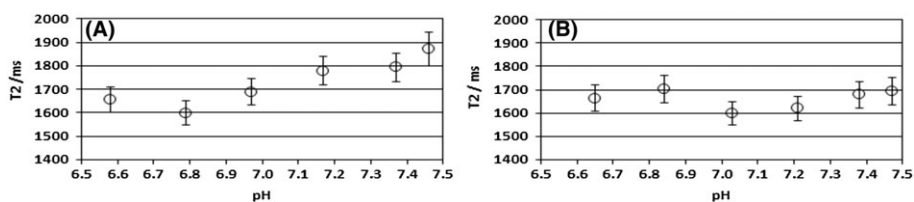


FIGURE 5 A, Transverse relaxation time (\pm sd of fit) of P_i in solutions of 20mM sodium phosphate (in 140mM NaCl; 0.4mM Na_2EDTA) as a function of pH. B, As in A with 5% fresh egg albumen added to the solutions. The complexing agent EDTA was added to minimize the influence of paramagnetic trace metals. Note the order of magnitude longer T_2 for P_i and the relative insensitivity of T_2 to pH

4 | DISCUSSION

The breast cancer spectra of Figure 2A clearly show higher PME to P_i and PME to PDE ratios as compared with the spectra from healthy fibroglandular breast tissue, indicative of enhanced phospholipid synthesis. The PDE metabolites in these spectra (breast cancer as well as healthy tissue) display a short T_2 component that we subscribe to mobile phospholipids¹⁰ in the form of GPC and GPE, as these signals disappear in the noise after the second echo. The aqueous PDE signals GPC and GPE remain visible at longer echo times. Patient spectra show a somewhat larger PCr signal than spectra from healthy volunteers. The PCr signal is due to voxel bleeding from the pectoralis muscle. On average, patient tumor voxels are located closer to the pectoralis muscle than the voxels chosen in the healthy volunteers that were closest to the nipple. The P_i signal in the breast cancer spectra decreases faster with echo time than the P_i signal in the spectra of healthy breast tissue. In fact, the apparent T_2 of P_i in breast cancer tissue is less than half that in healthy breast tissue, as can be observed from Figures 3 and 4, while the apparent T_2 of the other ^{31}P metabolites does not differ significantly between breast cancer and healthy tissue. As tumor tissue often shows a lower pH than healthy tissue, one may suspect the halved T_2 of P_i in breast cancer to be pH related. However, the phantom measurements of T_2 (Figure 5A and 5B) of P_i indicate that the shorter T_2 of P_i in breast cancer tissue is probably *not* caused by a general pH effect on the T_2 of P_i and/or a pH dependent general P_i -protein interaction, as the influence of pH and general protein interaction on the T_2 of P_i is only minor (Figure 5A and 5B). A possible mechanism for the apparent T_2 shortening effect of P_i in breast cancer tissue could be up-regulated glycolysis. This leads to the exchange of P_i with γ -ATP via the fully reversible Steps 6 and 7 of the glycolytic pathway as shown in Figure 1. It should be noted here that the exchange of P_i with γ -ATP is too slow to be of significance for shortening the T_2 of P_i . For instance, the exchange rate of $P_i \leftrightarrow \gamma$ -ATP in the brain is 0.2 s^{-1} ,^{15,16} and in resting muscle it is 0.06 s^{-1} .¹⁷ It is the reversible interaction with the GAPDH enzyme, which forms part of the pathway of P_i exchange with γ -ATP (Figure 1), that causes the apparent T_2 shortening of P_i . Although the exchange from P_i to γ -ATP and vice versa is relatively slow, the reversible interaction of P_i with GAPDH can be very fast (the maximum enzymatic capacity of GAPDH can be several hundred millimoles per minute depending on the tissue). Only a small fraction of the interactions of P_i with the GAPDH enzyme leads to the actual formation of ATP via this pathway. Likewise, only a small fraction of the interactions of ATP with the PGK enzyme leads to the formation of 1,3-DPG and subsequently to P_i via GAPDH.

When the exchange of P_i with GAPDH is faster than the transverse relaxation of P_i , this will lead to a reduction of signal over the echoes and thereby leads to an apparently lower T_2 value.

The measured apparent T_2 of P_i is an average value over intracellular and extracellular compartments, which are difficult to distinguish based on a subtle chemical shift difference (best viewed in final echo where signal levels seem comparable). Higher fields, or better B_0 shimming, may distinguish these P_i compartments better, yet the GAPDH enzyme is found intracellularly as well as extracellularly⁵ and can thus affect the apparent T_2 of P_i in both compartments. Up-regulated glycolysis is corroborated by the average GAPDH gene expression in breast cancer, which is over four times higher than in normal breast tissue.¹⁸ Song et al. even reported an increase in GAPDH gene expression of a factor of 5 to 21.¹⁹ Enhanced expression of GAPDH is associated with breast cancer cell proliferation and tumor aggressiveness.²⁰

Notably, glycolytic conversion of glucose is also important in muscle metabolism at rest¹⁷ and in the brain, where short transverse relaxation times for P_i are encountered as well. Muscle and brain tissue are among the tissues with the highest GAPDH mRNA expression, while healthy breast tissue has the lowest expression.²¹ The reported T_2 of P_i in muscle at rest at 7 T is around 100 ms (comparable to the T_2 value of P_i in breast cancer tissue), which is substantially shorter than the T_2 values for PCr and the PDEs in muscle.²² Recently, we measured the transverse relaxation times of the PMEs, PDEs and P_i in the healthy human brain at 7 T. In that study we also found a short relaxation time of P_i , only $86 \pm 2 \text{ ms}$.²³

The present study has several limitations. The breast cancerous lesions were all relatively small and therefore SNR of the spectra of the individual patients was too low to carry out T_2 fitting of metabolites. To enhance SNR and the reliability of T_2 fitting of ^{31}P metabolites, the breast cancer spectra of the patient group were averaged. To reduce voxel bleeding, Hanning filtering was performed before analysis, which increases the nominal voxel size by a factor of 1.78 in all spatial dimensions.²⁴ Although the voxels for which spectra were analyzed were carefully positioned around the cancerous lesions, some partial volume effect with healthy tissue is inevitable. However, with the proposed T_2 shortening mechanism of P_i , a mixture of cancerous and healthy fibroglandular tissue would lead to an increase in T_2 of P_i with increasing healthy tissue, contrary to the effect that we have measured. Considering the large voxel size and the relatively low density of glandular breast tissue in these older women, it was not possible to do an analysis of healthy glandular tissue with the unilateral setup that was used. An analysis of the data on GAPDH expression from the human protein atlas²⁵ in aging healthy fibroglandular breast tissue shows an average increase in GAPDH expression of 20% from women ranging between 25 and 65 years. Considering the difference in average age between the healthy volunteer group (26 years) and the patient group (59 years) it is to be expected that healthy breast tissue of the elderly patient group shows a shorter T_2 of P_i than that of the younger healthy volunteer group. However, the increase in GAPDH expression due to ageing is only minor as compared with the increased GAPDH expression as a consequence of breast cancer, where an average increase of a factor of 4 has been reported.¹⁸

Definite proof for the proposed T_2 shortening of P_i due to up-regulated GAPDH expression (and glycolysis) could be obtained from comparing multi-echo ^{31}P MR spectra of knock down GAPDH breast cancer xenografts with non-modified breast cancer xenografts.

In conclusion, the apparent transverse relaxation time of P_i in breast cancer tissue is less than half that in healthy fibroglandular tissue. The effect is most likely caused by an up-regulation of GAPDH expression (and glycolysis) in breast cancer tissue that leads to fast interaction of P_i with GAPDH, which is also seen in muscle tissue and brain tissue, with high GAPDH expression and similar short T_2 values for P_i .

FUNDING INFORMATION

This study was sponsored by Alpe d'Huzes UU2013-6302 and the Nederlandse Organisatie voor Wetenschappelijk Onderzoek VENI-JW-016.148.002.

REFERENCES

1. Glunde K, Bhujwala ZM, Ronen SM. Choline metabolism in malignant transformation. *Nat Rev Cancer*. 2011;11:835-848.
2. Podo F. Tumour phospholipid metabolism. *NMR Biomed*. 1999;12:413-439.
3. Sakurai H, Mitsuhashi N, Murata O, et al. Early radiation effects in highly apoptotic murine lymphoma xenografts monitored by ^{31}P magnetic resonance spectroscopy. *Int J Radiat Oncol Biol Phys*. 1998;41:1157-1162.
4. van der Kemp WJM, Stehouwer BL, Luijten PR, van den Bosch MAAJ, Klomp DWJ. Detection of alterations in membrane metabolism during neoadjuvant chemotherapy in patients with breast cancer using phosphorus magnetic resonance spectroscopy at 7 Tesla. *SpringerPlus*. 2014;3:634.
5. Gatenby RA, Gillies RJ. Why do cancers have high aerobic glycolysis? *Nat Rev Cancer*. 2004;4:891-899.
6. Seidler NW. *GAPDH: Biological Properties and Diversity (Advances in Experimental Medicine and Biology 985)*. Springer; 2013.
7. Weber JP, Bernhard SA. Transfer of 1,3-diphosphoglycerate between glyceraldehyde-3-phosphatedehydrogenase and 3-phosphoglycerate kinase via an enzyme-substrate-enzyme complex. *Biochemistry*. 1982;21:4189-4194.
8. Tomokuni Y, Goryo K, Katsura A, et al. Loose interaction between glyceraldehyde-3-phosphate dehydrogenase and phosphoglycerate kinase revealed by fluorescence resonance energy transfer-fluorescence lifetime imaging microscopy in living cells. *FEBS J*. 2010;277:1310-1318.
9. Scrutton MC, Utter MF. The regulation of glycolysis and gluconeogenesis in animal tissues. *Annu Rev Biochem*. 1968;37:249-302.
10. van der Kemp WJ, Stehouwer BL, Runge JH, et al. Glycerophosphocholine and glycerophosphoethanolamine are not the main sources of the in vivo ^{31}P MRS phosphodiester signals from healthy fibroglandular breast tissue at 7 T. *Front Oncol*. 2016;6:29.
11. Van der Kemp WJM, Boer VO, Luijten PR, Stehouwer BL, Veldhuis WB, Klomp DW. Adiabatic multi-echo ^{31}P spectroscopic imaging (AMESING) at 7 T for the measurement of transverse relaxation times and regaining of sensitivity in tissues with short T_2 values. *NMR Biomed*. 2013;26:1299-1307.
12. Naressi A, Couturier C, Devos JM, et al. Java-based graphical user interface for the MRUI quantitation package. *Magn Reson Mater Phys Biol Med*. 2001;12:141-152.
13. Vanhamme L, van den Boogaart A, Van Huffel S. Improved method for accurate and efficient quantification of MRS data with use of prior knowledge. *J Magn Reson*. 1997;129:35-43.
14. van der Kemp WJM, Stehouwer BL, Boer VO, Luijten PR, Klomp DWJ, Wijnen JP. Proton and phosphorus magnetic resonance spectroscopy of the healthy human breast at 7 T. *NMR Biomed*. 2017;30.
15. Ren J, Sherry AD, Malloy CR. Efficient ^{31}P band inversion transfer approach for measuring creatine kinase activity, ATP synthesis, and molecular dynamics in the human brain at 7 T. *Magn Reson Med*. 2017;78:1657-1666.
16. Ren J, Sherry AD, Malloy CR. ^{31}P -MRS of healthy human brain: ATP synthesis, metabolite concentrations, pH, and T_1 relaxation times. *NMR Biomed*. 2015;28:1455-1462.
17. Kemp GJ, Brindle KM. What do magnetic resonance-based measurements of $\text{Pi} \rightarrow \text{ATP}$ flux tell us about skeletal muscle metabolism? *Diabetes*. 2012;61:1927-1934.
18. Isidoro A, Casado E, Redondo A, et al. Breast carcinomas fulfill the Warburg hypothesis and provide metabolic markers of cancer prognosis. *Carcinogenesis*. 2005;26:2095-2104.
19. Song MN, Moon PG, Lee JE, et al. Proteomic analysis of breast cancer tissues to identify biomarker candidates by gel-assisted digestion and label-free quantification methods using LC-MS/MS. *Arch Pharm Res*. 2012;35:1839-1847.
20. Révillion F, Pawlowski V, Hornez L, Peyrat JP. Glyceraldehyde-3-phosphate dehydrogenase gene expression in human breast cancer. *Eur J Cancer*. 2000;36:1038-1042.
21. Barber RD, Harmer DW, Coleman RA, Clark BJ. GAPDH as a housekeeping gene: analysis of GAPDH mRNA expression in a panel of 72 human tissues. *Physiol Genomics*. 2005;21:389-395.
22. Bogner W, Chmelik M, Schmid AI, Moser E, Trattng S, Gruber S. Assessment of ^{31}P relaxation times in the human calf muscle: a comparison between 3 T and 7 T in vivo. *Magn Reson Med*. 2009;62:574-582.
23. van der Kemp WJM, Klomp DWJ, Wijnen JP. ^{31}P transverse relaxation times of phosphomonoesters, phosphodiesters and inorganic phosphate in the human brain at 7 tesla. *Magn Reson Med*. 2018;80:29-35.
24. Pohmann R, von Kienlin M. Accurate phosphorus metabolite images of the human heart by 3D acquisition-weighted CSI. *Magn Reson Med*. 2001;45:817-826.
25. Uhlén M, Fagerberg L, Hallström BM, et al. Proteomics. Tissue-based map of the human proteome. *Science*. 2015;347, 1260419.

How to cite this article: van der Kemp WJM, van der Velden TA, Schmitz AM, et al. Shortening of apparent transverse relaxation time of inorganic phosphate as a breast cancer biomarker. *NMR in Biomedicine*. 2019;32:e4011. <https://doi.org/10.1002/nbm.4011>